Natural discretization of pedestrian movement in continuous space

Michael J. Seitz and Gerta Köster
Department of Computer Science and Mathematics, Munich University of Applied Sciences, 80335 Munich, Germany
(Received 27 July 2012; published 15 October 2012)

Is there a way to describe pedestrian movement with simple rules, as in a cellular automaton, but without being restricted to a cellular grid? Inspired by the natural stepwise movement of humans, we develop a model that uses local discretization on a circle around virtual pedestrians. This allows for movement in arbitrary directions, only limited by the chosen optimization algorithm and numerical resolution. The radii of the circles correspond to the step lengths of pedestrians and thus are model parameters, which must be derived from empirical observation. Therefore, we conducted a controlled experiment, collected empirical data for step lengths in relation with different speeds, and used the findings in our model. We complement the model with a simple calibration algorithm that allows reproducing known density-velocity relations, which constitutes a proof of concept. Further validation of the model is achieved by reenacting an evacuation scenario from experimental research. The simulated egress times match the values reported for the experiment very well. A new normalized measure for space occupancy serves to visualize the results.

DOI: 10.1103/PhysRevE.86.046108 PACS number(s): 89.40.−a, 45.70.Vn

I. INTRODUCTION

There are many approaches to modeling pedestrian dynamics [1–3], among which cellular automata and social force models are particularly well established. In cellular automata, originally employed in traffic models [4,5], virtual pedestrians move on a fixed lattice of cells [6]. Cellular automata models based on a floor field have been extended to capture various characteristics of crowd movement [7–10]. The crowd dynamic strongly depends on the chosen shape of cells in two ways: First, pedestrians are represented by the cells. That means the dimension of cells is also the dimension of pedestrians' torsos. Since all cells are identical, there cannot be any variation in size and shape among different individuals. Compression of individuals is also impossible, contrary to what must be expected in dense crowds. Secondly, pedestrians step from cell to cell. Such stepwise movement seems natural and desirable but, on a cellular grid, it does not allow for movement in arbitrary directions. There is no reasonable solution known to the authors that solves the first issue. The second issue leads to several problems that can be dealt with at a price [11]: additional complexity must be introduced into the model that does not reflect natural phenomena, but is necessary to overcome unnatural phenomena generated *by* the model. On the plus side, cellular automata use intuitive rules to update the system states that can be chosen to match human choices closely. Hence, despite the obvious disadvantages, good results can be achieved within a certain range of applications.

Social force models have the advantage of operating in continuous space and time [12,13]. They are inspired by Newtonian mechanics and compute acceleration in dependence of repulsive and attractive forces. Unfortunately this introduces phenomena, like inertia or a tendency to oscillatory movement, that are unnatural to pedestrian movement. Also, overlapping is not excluded and must be dealt with, again, at the cost of introducing further complexity (see discussion in [14,15]). Finally, when introducing more advanced aspects of human behavior, like the coherence of social groups, it becomes more difficult to properly calibrate the model [16]. In a recent approach [17] the social force model is restricted to dense crowds, where the dynamics are assumed to be dominated by physical mechanisms, while cognitive heuristics are used to determine movement in sparse crowds.

The objective of this paper is to build a model that combines the advantages of both models without suffering from the disadvantages. We wish to maintain the stepwise movement of the cellular automaton. Even more importantly, we seek a rule based approach as we find it in both cellular automata and cognitive heuristics. But we do not want to be bound to a rigid spatial grid. Other works with related objectives could achieve reasonable results for various simulation aspects [18,19] but do not show all the characteristics we wish to capture.

The paper is structured as follows: We describe the model and the fundamental idea of discretizing space locally on a circle around each moving pedestrian (Sec. II). Then we report measurements of step lengths in relation with the velocity from a controlled experiment (Sec. III). In the following section (Sec. IV) we validate the model by showing how it can be calibrated to a given density-speed relationship. Subsequently (Sec. V) we use the calibrated model to conduct simulations according to a controlled experiment and describe a normalized measure for the occupation of space to visualize the outcome. Finally the results and the direction of possible future work are discussed.

II. MODEL

The model proposed here is partially based on ideas known from cellular automata, namely, the use of attractive and repulsive potentials when choosing a direction of movement for pedestrians [11]. The speed of movement is determined independently. Each pedestrian has a desired speed, that is, the speed the pedestrian would like to move at on a free plane. Speed adjustments are possible; for instance pedestrians slow down in dense crowds or adjust their speed in order to maintain a group structure [20,21].

A. Attractive and repulsive potentials

An attractive force to the target is realized with a potential that represents the propagation of a wave front and is implemented as a floor field [22]. This is very important in order to make pedestrians successfully skirt obstacles. If we used the Euclidian distance along the line of sight to the target as an attractive potential, pedestrians would get trapped by concave obstacles. The floor field is computed with Sethian's fast marching algorithm on a two-dimensional grid [23,24]. We use bilinear interpolation to obtain a target potential value $P_t(x)$ for an arbitrary point $x \in \mathbb{R}^2$ in the plane.

In contrast to cellular automata, the proposed model does not represent pedestrians by cells, nor do they have to move from cell to cell. Pedestrians are represented by their position and extension in space. For simplicity we use the same circular shape for each person at this point. Other shapes, such as ellipses, that better match the human torso, or even individualized shapes for different body sizes can easily be incorporated in the model. The movement is driven by the desired speed and direction of the pedestrian. After each time step pedestrians are informed about how much time has elapsed and decide whether to move or not to achieve their desired speed. The desired speed is a fixed attribute of each pedestrian, but could also be adapted if the motivation to approach the target increases or decreases. Note that this model does not take into account acceleration or inertia, although it was shown to be a measurable factor for pedestrian movement [16].

In addition to the attractive potential of the target we use two types of repulsive potentials. The first one is carried around each pedestrian:

$$P_{p,i}(x) = \begin{cases} \mu_p & \text{if } \delta_{p,i}(x) \leqslant g_p \\ \nu_p \times \exp[-a_p \times \delta_{p,i}(x)^{b_p}] & \text{if } g_p < \delta_{p,i}(x) \leqslant g_p + h_p. \\ 0 & \text{else} \end{cases} \tag{1}$$

$P_{p,i}(x)$ is the repulsive potential of pedestrian i affecting another pedestrian at position x. It depends on the Euclidian distance $\delta_{p,i}(x)$ from x to the center of pedestrian i. The diameter of pedestrian torsos is denoted by g_p. If $\delta_{p,i}(x) \leqslant g_p$, that is, if the torso of a pedestrian at position x overlapped with the torso of pedestrian i, we set the potential at a high level μ_p to assure that stepping on another pedestrian's torso is less attractive than any other unoccupied position. For simplicity μ_p is chosen to be a constant value. We also cut off the fast fading potential outside the torso at distance $g_p + h_p$ for better computational speed and steadier movement of pedestrians, which also leads to a more stable crowd movement.

Additional parameters are a_p, b_p, and ν_p. We use $\mu_p = 1000$, $\nu_p = 0.4$, $a_p = 1$, $b_p = 0.2$, $g_p = 0.4$, and $h_p = 1$, derived from careful visual validation to reproduce natural behavior. All distances are measured in meters. Note that more sophisticated potential functions could easily be introduced to fine tune the repulsions and allow for partial overlapping or even compression of the torso.

A similar formula with different parameters is used for repulsive potentials around obstacles:

$$P_{o,j}(x) = \begin{cases} \mu_o & \text{if } \delta_{o,j}(x) < g_p/2 \\ \nu_o \times \exp[-a_o \times \delta_{o,j}(x)^{b_o}] & \text{if } g_p/2 \leqslant \delta_{o,j}(x) \leqslant h_o. \\ 0 & \text{else} \end{cases} \tag{2}$$

$P_{o,j}(x)$ is the repulsive potential induced by obstacle j, where $\delta_{o,j}(x)$ is the distance to the closest point of the obstacle from position x. Here we use $\mu_o = 10\,000$, $\nu_o = 0.2$, $a_o = 3$, $b_o = 2$, and $h_o = 6$. We would like to point out that, as of today, the effect of obstacles on pedestrians, such as the distance they keep in different situations, has not been investigated thoroughly. Hence our validation must again be restricted to visual comparison. The choice of μ_o ensures that pedestrians do not move to positions with $\delta_{o,j}(x) < g_p/2$ where the pedestrian torso would overlap with the obstacle.

If the obstacle potential were too strong, small corridors would be blocked by it. Therefore we choose a rather weak but far reaching potential. Both kinds of potentials ensure that pedestrians keep a distance from each other and do not walk too close to walls. This has been shown to be a emergent effect in experiments [16].

For each pedestrian l we form an aggregated potential that can be evaluated at any point in the plane:

$$P_l(x) = P_t(x) + \sum_{i=1, i\neq l}^{n} P_{p,i}(x) + \sum_{j=1}^{m} P_{o,j}(x), \tag{3}$$

with $n-1$ other pedestrians and m obstacles in the scenario. With this framework more complex aspects of pedestrian movement, such as group structures in crowds [20,21], can easily be carried over.

B. Natural discretization on local circles

So far we have values for the aggregated potential at all positions in the plane. The more repulsive the potential of a position is, the higher the value of the potential function. Thus $-P$ can be interpreted as a utility function for the pedestrian in which the points on the target have the highest utility with value zero. With this information we can use gradient descent methods to reach the minimum. Since the movement of pedestrians is naturally stepwise, we optimize locally for the next step. This results in a greedy algorithm without planning for future steps. At the same time, the floor field carries global information that takes into account the walking distance to the target around obstacles on a scenario wide level. Thus local minima cannot trap pedestrians who follow a greedy strategy. The only exceptions are temporary local minima created by potentials around other pedestrians. One way to resolve these

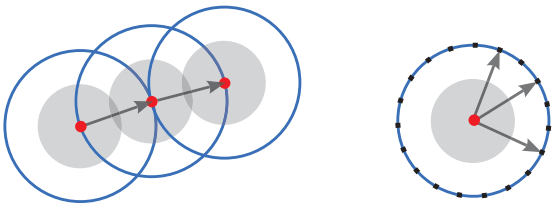

FIG. 1. (Color online) Left: sequence of three time steps $t = 1,2,3$. The pedestrian torso is depicted with the filled inner circle. The next position has to be on the step circle around the pedestrian. Right: discretization of the circle indicated by points. The three arrows represent three possible choices for the next step.

is to let pedestrian agglomerations slow down the propagation of the wavefront when computing the floor field [22].

We further simplify by taking into account only positions that lie on a circle with radius r around the pedestrian. The radius r corresponds to the step length of each pedestrian. This reduces the utility function to a one-dimensional periodic function that can be minimized very easily and cost effectively. A simple optimization algorithm is to consider q equidistant points on a circle and find the one with the lowest potential value. This is computationally efficient if q is rather small, say between 8 and 32. This kind of discretization would lead to artifacts, if the considered points always had the same position on the circle. Therefore we disturb the positions on the circle with a small noise term:

$$\varphi = \frac{2\pi}{q}(k+u), \quad u \sim U(0,1), \tag{4}$$

where u is a random value uniformly distributed between 0 and 1. Finally we choose the position with the smallest value $P(x_k)$ for $k = 0,\ldots,q$. With $x_k = (x_{1,k},x_{2,k})$ we have

$$x_k = x_0 + r \times (\cos(\varphi), \sin(\varphi)), \tag{5}$$

for $k = 1,\ldots,q$ and $x_0 = (x_{1,0},x_{2,0})$ as the current position of the pedestrian. Note that the pedestrian can also remain at the current position x_0, if it has the smallest potential value. Figure 1 illustrates the key aspects of this model. If we choose only six possible points on the circle, that is $q = 6$ in Eq. (4), and set the random value $u = 0$, the model reproduces movement in a cellular automaton with hexagonal cells. Four directions yield the movement in a rectangular cellular automaton grid with von Neumann neighborhood. Two concentric circles with radii r and $\sqrt{2}r$ and four directions on each circle reproduce the movement according to the Moore neighborhood (see Fig. 2).

Other optimization methods on the circle are also possible. For instance, one could use Brent's method [26], which does not require the evaluation of derivatives. Furthermore less strict constraints could be set. Several circles with different radii would allow for different step lengths. Two-dimensional optimization within the circle would allow any step length smaller than the radius. With the latter, more complex optimization choice, the model allows for movement in truly continuous space, only limited by the numerical resolution.

Positions are updated sequentially so that collisions do not occur. The effect of the sequential update disappears if, in theory, the length of the simulation time step goes to zero. That is, every pedestrian moves exactly at the time the next step is feasible according to the current velocity. Thus, to prevent

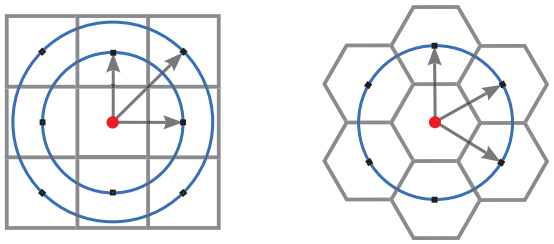

FIG. 2. (Color online) Movement in cellular automata with squares (left) and hexagons (right) replicated with circle discretization. For this purpose the random disturbance of the position has to be turned off and only positions on the circle that match the center of cells must be allowed.

possible effects of the sequential update, one can choose a small value for the time step. Possible effects of a greater value could be microscopic agglomerations of pedestrians. For instance, a pedestrian who would be allowed to move after the pedestrian in front of him or her, in theory, might move first due to the sequential update and thus bump into the pedestrian in front. This would not happen if the pedestrian in front had moved first.

With this model we obtain very realistic trajectories for the movement of individual pedestrians (see Fig. 3).

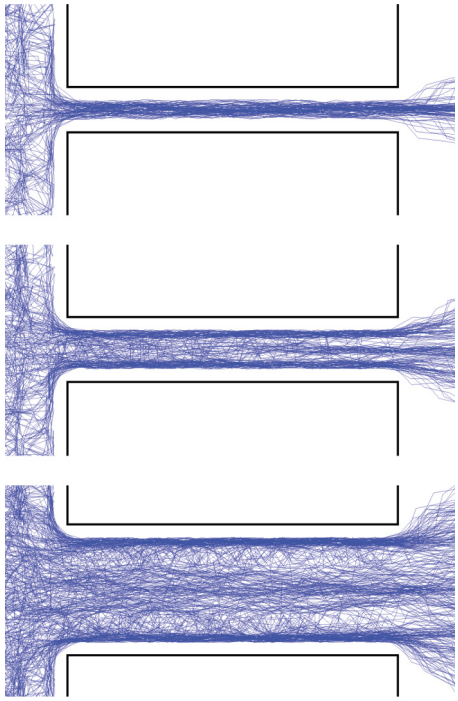

FIG. 3. (Color online) Accumulated trajectories for simulated pedestrians passing from left to right through a corridor with length 5 m and different widths. The first scenario (top) has a corridor width of 0.7 m. Pedestrians cannot walk next to each other and therefore form one lane. In the second scenario (middle), with a corridor width of 1 m, pedestrians form two distinctive lanes at the boundaries and a third in the middle visible at the end of the corridor. In the last scenario (bottom), with a corridor width of 2 m, the accumulated trajectories show two distinctive and one or two fuzzy lanes in the middle. Very similar trajectories were observed by empirical researchers [25].

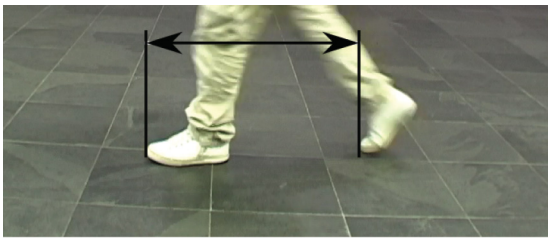

FIG. 4. (Color online) Screen capture of the video footage used to determine the step lengths. The length is measured from toecap to toecap while the relevant part of the foot touches the ground. When subjects are running it is necessary to take the measurement for each foot at different moments, because only one foot touches the ground at a time.

III. EMPIRICAL MEASUREMENT OF STEP LENGTHS

With discretization on a circle the radius r, which represents the step length of a pedestrian, is a crucial parameter. Several studies investigate the relation of step lengths to other parameters, and suggest a strong dependence on the speed [27–29]. If we assume that humans minimize the metabolic energy cost while walking, the relation can also be investigated as an optimization problem [30]. To collect data for a wide range of speeds we carried out a controlled experiment. Fourteen students were asked to walk, jog, and run a distance of 12 m several times. Each subject walked on his or her own, thus excluding any interaction among them. We measured the time it took the subjects to cover the distance. The middle section of the path was recorded with a video camera. This video footage was then analyzed to retrieve the step lengths (see Fig. 4).

We investigate whether there is a correlation between velocity and step lengths. For this purpose a linear regression with the step length as response variable and the speed as explanatory variable is conducted:

$$y_{\text{step}} = \beta_0 + \beta_1 \times x_{\text{speed}} + \epsilon. \tag{6}$$

The error term ϵ is assumed to be normally distributed. The regression yields the estimates $\hat{\beta}_0 = 0.462$ (standard error $=$ 0.021) and $\hat{\beta}_1 = 0.235$ (s.e. $= 0.012$) for the data with walking behavior (see Fig. 5). Both estimates are highly significant (t-test, $p < 0.001$). The standard error of the regression is $\hat{\sigma} = 0.036$ on 82 degrees of freedom. This result is in very good agreement with an older study [27].

The data show a nonlinear trend in a scatter plot, when taking into account jogging and running. Hence we propose a second regression model for the whole data set with a quadratic term for the speed (see Fig. 6):

$$y_{\text{step}} = \beta_0 + \beta_1 \times x_{\text{speed}} + \beta_2 \times x_{\text{speed}}^2 + \epsilon. \tag{7}$$

This time we get $\hat{\beta}_0 = 0.218$ (s.e. $= 0.04$), $\hat{\beta}_1 = 0.433$ (s.e. $=$ 0.028), and $\hat{\beta}_2 = -0.032$ (s.e. $= 0.004$), again, with high significance for all estimates (t-test, $p < 0.001$). The standard error of the regression is $\hat{\sigma} = 0.07$ on 107 degrees of freedom.

We conclude that the step length strongly depends on the speed of movement. At first the step length increases linearly with the speed, but does not increase any further after about 4 m/s. This also matches other reported diagrams [31,32]. Interestingly, taking the body height of the subjects into account does not improve the regression model significantly

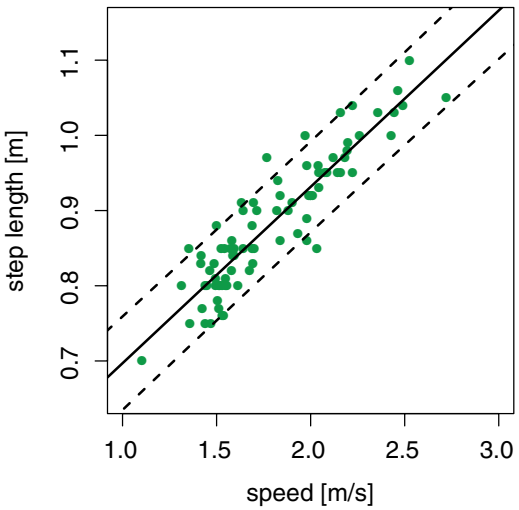

FIG. 5. (Color online) Linear regression between step length and speed for walking behaviors. Walking behaviors included normal and fast walking. The slope of the regression suggests a strong linear dependence. The dashed lines indicate the 0.9 prediction interval.

(t-test, $p = 0.334$). Clearly the data may be biased, because the subjects do not represent an arbitrary crowd of pedestrians. Also the sample is rather small in general, and sparse at high and low speeds. Nevertheless, the results seem conclusive and the data can be extended for other populations in order to obtain a more representative concept.

IV. DENSITY-SPEED RELATION

The density-speed relation, given by fundamental diagrams, is one of the most important benchmark tests for crowd simulations, although there is an ongoing discussion on correct shapes and measurement methods [16,25,33,34]. We conduct simulations dedicated to measuring the density-speed relation. Subsequently we calibrate according to a specific fundamental

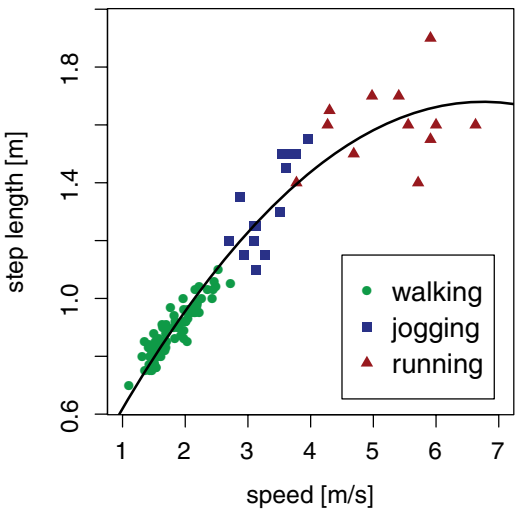

FIG. 6. (Color online) Linear regression with a quadratic speed term for the whole data set, including running and jogging. The dependence shows significant nonlinear behavior. At high speeds one has to assume higher variance and thus heteroscedasticity.

diagram, which is a proof of concept for the calibration to an arbitrary density-speed relation. Since fundamental diagrams are seen as an aggregated expression of socio-cultural characteristics, a model should be able to calibrate according to any reasonable measured fundamental diagram [35,36].

A. Simulation parameters and measurement methodology

For comparability we use parameters given by Weidmann [31] for the mean ($\mu_v = 1.34$ m/s) and standard deviation ($\sigma_v = 0.26$ m/s) of the desired walking speed v. Obviously this does not reflect our measurement of the mean speed in the controlled experiment, which may be due to the differences in the populations that were considered. However, we use Weidmann's mean for later consistent comparison of our simulation measurements regarding the relation between density and speed. The desired walking speed v_i for individual i is then chosen according to a truncated normal distribution. It is necessary to truncate the distribution in order to prevent implausibly small, even negative, or implausibly big values that do not reflect natural behavior. Together we have

$$v_i \sim N_{\text{tr}}(\mu_v,\sigma_v;-\sigma_v M,\sigma_v M), \tag{8}$$

with $N_{\text{tr}}(\mu_v,\sigma_v;-\sigma_v M,\sigma_v M)$ denoting a normal distribution that is truncated at $-\sigma_v M$ and $\sigma_v M$. For this we draw normally distributed values with mean μ_v and standard deviation σ_v. If the absolute value exceeds $M\sigma_v$, we discard the value and draw again. In the following we use $M = 2$, that is, two times the standard deviation and thus $\sigma_v M = 0.52$ as cutoff. Therefore we obtain values from 0.82 to 1.86 m/s as desired walking speeds. We want to stress that, in general, parameters should be set depending on the scenario investigated and the available data.

The step length r is chosen according to the estimates of the regression for walking behavior with $\beta_0 = 0.462$ and $\beta_1 = 0.235$ [Sec. III, Eq. (6)]. The individual expected step length μ_{r_i} is therefore determined by the individual desired speed v_i with

$$\mu_r(v_i) = \beta_0 + \beta_1 \times v_i. \tag{9}$$

Again we use a truncated normal distribution with $M = 2$ to determine the individual step length r_i. Here we obtain values from $\mu_r(v_i) - 0.072$ to $\mu_r(v_i) + 0.072$ m for the step length of individual i:

$$r_i \sim N_{\text{tr}}(\mu_r(v_i),\sigma_r;-\sigma_r M,\sigma_r M). \tag{10}$$

In scenarios with higher desired speeds of pedestrians, one should consider the regression with the quadratic term [Sec. III, Eq. (7)]. A further sophistication could be the dynamic adaption of step lengths during the simulation according to the current speed. In our case we only consider the desired speed of individuals and then fix the step length for the whole simulation.

We choose $q = 18$ as the number of possible positions on the circle. A higher value would yield smoother movement of pedestrians, but would also slow down computational speed. The simulation time step for this experiment is set to the rather big value of 0.5 s, again to speed up computation.

Two values have to be captured during simulation to obtain a fundamental diagram: the density and the speed. We measure as follows: First we determine the speed of each pedestrian at a given simulation time step and then average over all pedestrians within a certain measurement area. Since the model is discretized in time and space, we use the history of movement for each pedestrian. We take the distance covered towards the target within the last five steps and divide it by the simulation time that elapsed. In order to capture the density, we employ Voronoi diagrams [25,37] and use the formula

$$D_v = \frac{N}{\sum_{i=1}^{N} |A_i|}, \tag{11}$$

where D_v is the density in the measurement area, N the number of pedestrians within it, and $|A_i|$ the size of the Voronoi cell allocated to pedestrian i. The measurement with Voronoi diagrams yields smoother curves for density over time and thus is superior to other methods [25,37]. When the measurement is not averaged over an area, other methods might be more suitable (see Sec. V).

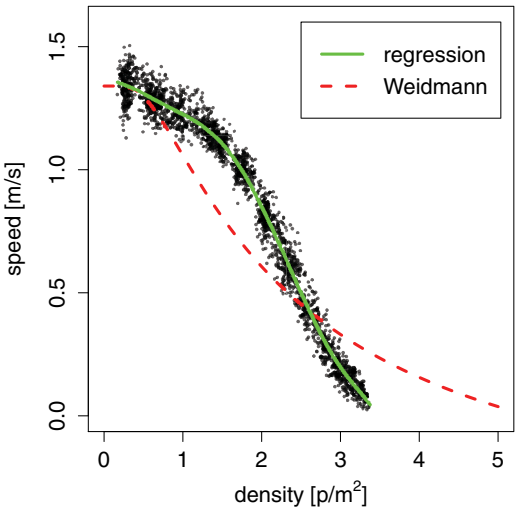

FIG. 7. (Color online) Scatterplot of the density-speed relation with a torso diameter of 0.4 m. The solid (green) line is a spline regression through the measurement points. The dashed (red) line is the theoretical relation given by Weidmann [31].

B. Comparative measurements and adaptive calibration

The scenario in which we measure the density-speed relation is a corridor of width 4 m and length 50 m. All pedestrians walk in one direction. When they reach the target, which is located at the end of the corridor, they are instantly moved back to the beginning of the corridor at the same position widthwise.

After a settling time of 100 s measurements are taken after each time step within an area in the middle of the corridor that is 10 m long and 4 m wide. The speed for each time step is then averaged over all pedestrians within the field and the density calculated according to Eq. (11).

To obtain densities for the full range of possible speeds, we conduct various simulation runs with an increasing number of pedestrians in the scenario until almost no movement is possible. Figure 7 shows the density-speed relation as a scatterplot in comparison to the theoretical curve given by Weidmann [31]. The decrease of speed with increasing density is reproduced. The speed measured in the simulation converges

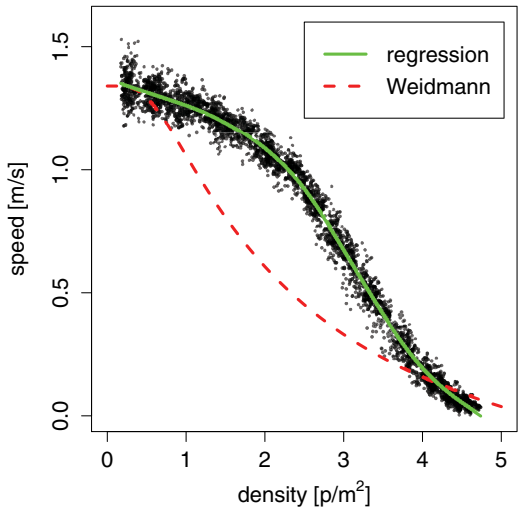

FIG. 8. (Color online) Density-speed relation with a torso diameter of 0.35 m.

to zero faster than the theoretical curve. When we reduce the diameter of pedestrians' torsos from 0.4 to 0.35 m to allow for higher densities (see Fig. 8), we get a good match at very high and very low densities, but exceed the theoretical speed systematically in between. Apparently real pedestrians react more strongly to high crowd densities than the virtual pedestrians of the model.

To remedy this, we introduce a local density measure for pedestrians to incorporate adaptive calibration: Pedestrians slow down when they walk into a dense crowd. For this we count other pedestrians more than 0.1 m ahead from the pedestrian's center, but not further away than 1.5 m. The number of pedestrians n_p in this proximity is then used to calculate the local density. If the speed of a pedestrian at a given local density exceeds the one given by the fundamental diagram, the pedestrian is not allowed to move for one time step. The result of the simulation for Weidmann's diagram is given in Fig. 9. Although the measurements do not match the curve exactly, it displays a good approximation. The

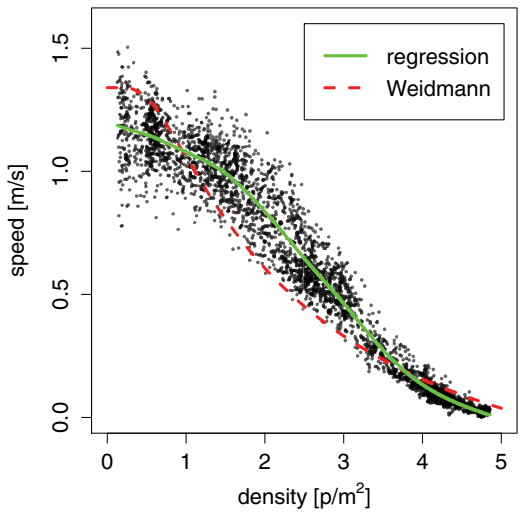

FIG. 9. (Color online) Density-speed relation with a torso diameter of 0.35 m and adaptive calibration.

calibration method is applicable to arbitrary fundamental diagrams. Furthermore the heteroscedasticity of the variance, that is, higher variance at low densities and low variance at high densities, seems reasonable.

V. SIMULATION STUDY AT A BOTTLENECK

One of the most important objectives in crowd research is the prediction of unpleasant, obstructive, or even dangerous situations. Some kind of density measure is usually employed for this purpose [21,34]. In Sec. IV we used Voronoi diagrams to measure the density-speed relationship in a measurement area. This method is very accurate and reasonable if the density is averaged over an area. For local densities, on the other hand, density measurements with Voronoi diagrams seem to be shortsighted: Only direct neighbors are considered, who contribute to the edges of the cell. More distant pedestrians, or a wall behind a neighbor, result in the same local density value as an open space around the neighbor. This does not reflect how crowded an individual feels in the situation. Therefore we use a Gaussian function to locally weight pedestrians with positions x_i at any fixed position z [34,38]:

$$f(x_i,z) := \frac{1}{2\pi R^2} \exp\left(-\frac{1}{2R^2}||x_i - z||^2\right). \qquad (12)$$

The parameter R controls the width of the Gaussian function; the smaller it is, the more weight is assigned to closer pedestrians. We choose $R = 0.7$ to get a smooth but sufficiently detailed resolution. The sum over all pedestrians

$$D_p(z) := S_p \sum_{i=1}^{n} f(x_i,z) \qquad (13)$$

is a measure for the local pedestrian density. The parameter S_p normalizes D_p to lie within the interval $[0,1]$. We choose S_p so that Eq. (13) attains the value 1 for a theoretical crowd packed at maximum density in all directions to infinity and 0 for an empty space. We argue as follows: Close-packed spheres in two dimensions correspond to a Voronoi diagram with identical hexagonal cells. Hence, in the close-packed case, each pedestrian in our model occupies a hexagonal area of size $A_i = 2\sqrt{3}(g_p/2)^2$ where g_p is the torso diameter. The sum of Eq. (13) can then be interpreted as the Riemann sum of Eq. (12). The Riemann integral of Eq. (12) is 1. Hence, if we

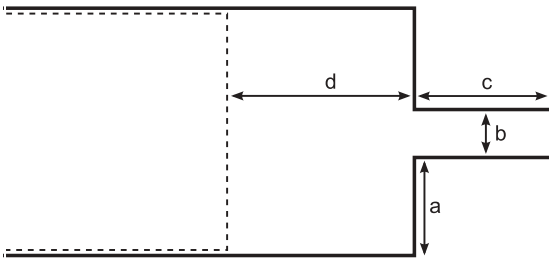

FIG. 10. Schematical depiction of the scenario following a controlled experiment [39]. In the first scenario the lengths $a = 3$ m, $b = 2$ m, $c = 4$ m, $d = 12$ m are set, and in the second scenario the lengths $a = 3.5$ m, $b = 1$ m are set. Pedestrians are placed in the area surrounded with the dashed line. The target is placed on the right, outside of the corridor.

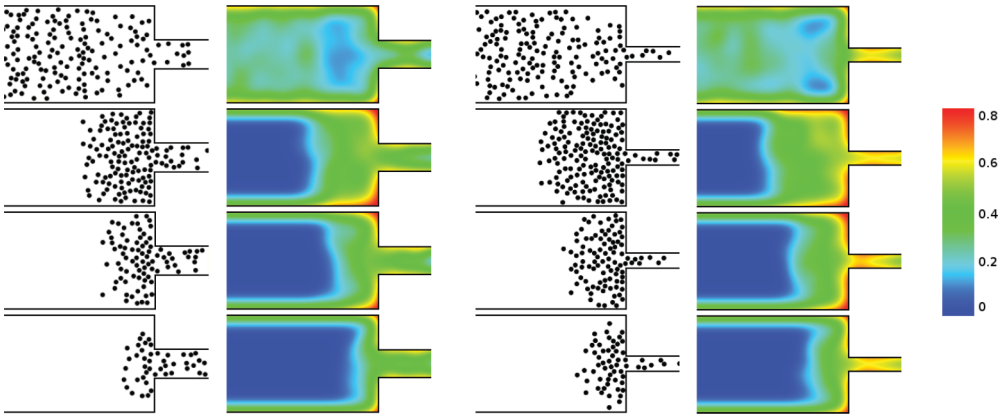

FIG. 11. (Color online) Comparative depiction of two scenarios with 180 virtual pedestrians leaving a room through a bottleneck. Left: scenario with bottleneck width of 2 m displayed after 10, 20, 30, and 40 s (from top to bottom) after the beginning of the egress. Right: scenario with bottleneck width of 1 m after 10, 20, 50, and 70 s. Each situation is depicted twice, in the left column with the positions of the pedestrians and in the right column with the local degree of occupation. Dark areas (blue or read) represent the extremes, that is, very high or low occupation. The dark (blue) areas in the middle of the room indicate very low occupation. The dark (red) areas at the corners indicate very high occupation. Although values of up to 1 would be possible in theory, only values of up to 0.8 were observed, hence the legend is limited by this value too.

let g_p go to zero, we get

$$\lim_{g_p \to 0} D_p(z) \times g_p^2 \sqrt{3}/2 = S_p \int_{\mathbb{R}^2} f(x,z) d^2x = S_p, \quad (14)$$

and thus $S_p = g_p^2 \sqrt{3}/2$ is suitable as the normalization factor. In addition we want to consider obstacles as occupied area. This leads away from the notion of pure pedestrian density, but it also seems unreasonable to ignore the restricting effects of walls. In this case we integrate the Gaussian function over the occupied areas O_i:

$$D_o(z) = \sum_{i=1}^{m} \int_{O_i} f(x,z) d^2x. \quad (15)$$

The resulting local measure is calculated as the sum $D_l(z) = D_p(z) + D_o(z) \in [0,1]$. We want to stress that this is not a measure for pedestrians per square meter, but a measure of local occupation of space by pedestrians *and* obstacles. Therefore the space close to walls will not be regarded as free in the same way as unoccupied space in the middle of a room. Instead the measure reflects how restricted a person would feel if he or she was placed in such a position. Hence, in contrast to other density measures, the space close to walls is considered restricted to a certain level, even when there are no pedestrians.

We apply this measure for a simulation study that follows a controlled experiment [39]. The setup is described in Fig. 10. We simulate the scenario twice, once with a bottleneck of 2-m width and then again with 1-m width.

As in the original experiment, 180 pedestrians are placed in the room in each run. The evacuation times of 52 s for the first scenario and 104 s for the second scenario in the simulation match those reported for the controlled experiment closely [39]. The results of the measure for local occupation are given in Fig. 11. High occupation and thus potentially dangerous areas are detected in the corners for both scenarios. For the second scenario high occupation was found additionally in front of the bottleneck and in the corridor. Although pedestrians accumulate in front of the bottleneck, the measurement for local occupation does not show particularly high values in this area. This is due to the fact that walls are considered more restraining than other pedestrians. The density of pedestrians per square meter on the other hand is fairly high, which can be observed in the figures with the pedestrian positions (see Fig. 11).

VI. CONCLUSION

We described a new mathematical model for pedestrian movement that takes place in continuous space and is discretized in a way that reflects natural movement. The model is a solution to the previously unsolved problem of how to achieve natural grid-free trajectories without introducing social force type differential equations or complex steering behaviors [40]. It remains computationally efficient and allows for extensions to more complex human behavior, such as social group behavior, and to agent-type mechanisms [41]. Optimization methods allow us to find the best next step with respect to a floor field that describes the global strategy to skirt obstacles on the way to a target. The model can be calibrated to match fundamental diagrams, which is crucial, because different density-speed relations hold for different scenarios. A simulation study yields evacuation times matching those reported for controlled experiments, which further supports the model's validity. Because of its simplicity and flexibility the model could be used for many extensions and applications in various fields, like social sciences, safety science, and artificial intelligence.

ACKNOWLEDGMENTS

This work was partially funded by the German Federal Ministry of Education and Research through the project MEPKA on mathematical characteristics of pedestrian stream models (Grant No. 17PNT028).

[1] S. Gwynne, E. Galea, M. Owen, P. Lawrence, and L. Filippidis, Building Environment **34**, 741 (1999).

[2] X. Zheng, T. Zhong, and M. Liu, Building Environment **44**, 437 (2009).

[3] A. Smith, C. James, R. Jones, P. Langston, E. Lester, and J. Drury, Safety Science **47**, 395 (2009).

[4] K. Nagel, Phys. Rev. E **53**, 4655 (1996).

[5] K. Nagel, D. E. Wolf, P. Wagner, and P. Simon, Phys. Rev. E **58**, 1425 (1998).

[6] V. J. Blue and J. L. Adler, Transp. Res. Part B **35**, 293 (2001).

[7] C. Burstedde, K. Klauck, A. Schadschneider, and J. Zittartz, Physica A **295**, 507 (2001).

[8] A. Kirchner, H. Klüpfel, K. Nishinari, A. Schadschneider, and M. Schreckenberg, Physica A **324**, 689 (2003).

[9] C. M. Henein and T. White, Physica A **373**, 694 (2007).

[10] T. Ezaki, D. Yanagisawa, K. Ohtsuka, and K. Nishinari, Physica A **391**, 291 (2012).

[11] G. Köster, D. Hartmann, and W. Klein, in *Operations Research Proceedings 2010: Selected Papers of the Annual International Conference of the German Operations Research Society*, edited by B. Hu, K. Morasch, S. Pickl, and M. Siegle (Springer, Berlin, 2011), pp. 571–576.

[12] D. Helbing and P. Molnár, Phys. Rev. E **51**, 4282 (1995).

[13] D. Helbing, I. Farkas, and T. Vicsek, Nature (London) **407**, 487 (2000).

[14] M. Chraibi, A. Seyfried, and A. Schadschneider, Phys. Rev. E **82**, 046111 (2010).

[15] M. Chraibi, U. Kemloh, A. Schadschneider, and A. Seyfried, Networks Heterogeneous Media **6**, 425 (2011).

[16] M. Moussaïd, D. Helbing, S. Garnier, A. Johansson, M. Combe, and G. Theraulaz, Proc. R. Soc. B **276**, 2755 (2009).

[17] M. Moussaïd, D. Helbing, and G. Theraulaz, Proc. Natl. Acad. Sci. USA **108**, 6884 (2011).

[18] G. Antonini, M. Bierlaire, and M. Weber, Transp. Res. Part B **40**, 667 (2006).

[19] G. Baglietto and D. R. Parisi, Phys. Rev. E **83**, 056117 (2011).

[20] G. Köster, M. Seitz, F. Treml, D. Hartmann, and W. Klein, Contemporary Social Science **6**, 397 (2011).

[21] M. Moussaïd, N. Perozo, S. Garnier, D. Helbing, and G. Theraulaz, PLoS ONE **5**, e10047 (2010).

[22] D. Hartmann, New J. Phys. **12**, 043032 (2010).

[23] J. A. Sethian, Proc. Natl. Acad. Sci. USA **93**, 1591 (1996).

[24] J. A. Sethian, *Level Set Methods and Fast Marching Methods*, 2nd ed. (Cambridge University Press, Cambridge, 1999).

[25] A. Schadschneider and A. Seyfried, Networks Heterogeneous Media **6**, 545 (2011).

[26] R. Brent, *Algorithms for Minimization without Derivatives* (Prentice-Hall, Englewood Cliffs, 1973).

[27] C. Kirtley, M. Whittle, and R. Jefferson, J. Biomed. Eng. **7**, 282 (1985).

[28] D. W. Grieve and R. J. Gear, Ergonomics **9**, 379 (1966).

[29] L. Wolfson, J. Judge, R. Whipple, and M. King, J. Gerontol. A Biol. Sci. Med. Sci. **A50** (special issue), 64 (1995).

[30] A. D. Kuo, J. Biomech. Eng. **123**, 264 (2001).

[31] U. Weidmann, *Transporttechnik der Fussgänger*, Vol. 90 (Schriftenreihe des Institut für Verkehrsplanung, Transporttechnik, Strassen- und Eisenbahnbau, ETH Zürich, 1992).

[32] R. Margaria, *Biomechanics and Energetics of Muscular Exercise* (Oxford University Press, Oxford, 1976).

[33] A. Seyfried, B. Steffen, W. Klingsch, and M. Boltes, J. Stat. Mech. (2005) P10002.

[34] D. Helbing, A. Johansson, and H. Z. Al-Abideen, Phys. Rev. E **75**, 046109 (2007).

[35] U. Chattaraj, A. Seyfried, and P. Chakroborty, Advances Complex Systems **12**, 393 (2009).

[36] M. Davidich and G. Köster, Safety Science **50**, 1253 (2012).

[37] B. Steffen and A. Seyfried, Physica A **389**, 1902 (2010).

[38] M. Plaue, M. Chen, G. Bärwolff, and H. Schwandt, in *Photogrammetric Image Analysis*, Lecture Notes in Computer Science Vol. 6952, edited by U. Stilla, F. Rottensteiner, H. Mayer, B. Jutzi, and M. Butenuth (Springer, Berlin, 2011), pp. 285–296.

[39] J. Liddle, A. Seyfried, B. Steffen, W. Klingsch, T. Rupprecht, A. Winkens, and M. Boltes, arXiv:1105.1532v1.

[40] C. W. Reynolds, in *Proceedings of Game Developers Conference* (Miller Freeman Game Group, San Francisco, CA, 1999), pp. 763–782.

[41] B. E. Aguirre, S. El-Tawil, E. Best, K. B. Gill, and V. Fedorov, Contemporary Social Science **6**, 415 (2011).